Quantifying cross-shelf and vertical nutrient flux in the Coastal Gulf of Alaska with a spatially nested, coupled biophysical model

Albert J. Hermann [a,*], Sarah Hinckley [b], Elizabeth L. Dobbins [a], Dale B. Haidvogel [c], Nicholas A. Bond [a], Calvin Mordy [a], Nancy Kachel [a], Phyllis J. Stabeno [d]

[a] *Joint Institute for the Study of the Atmosphere and Ocean, University of Washington, P.O. Box 357941, Seattle, WA 98195, USA*
[b] *Alaska Fisheries Science Center, 7600 Sand Point Way N.E., Seattle, WA 98115, USA*
[c] *Institute of Marine and Coastal Sciences, Rutgers University, 71 Dudley Road, New Brunswick, NJ 08901-8521, USA*
[d] *Pacific Marine Environmental Laboratory, 7600 Sand Point Way N.E., Seattle, WA 98115, USA*

ARTICLE INFO

ABSTRACT

The Coastal Gulf of Alaska (CGOA) is productive, with large populations of fish, seabirds, and marine mammals; yet it is subject to downwelling-favorable coastal winds. Downwelling regions in other parts of the world are typically much less productive than their upwelling counterparts. Alternate sources of nutrients to feed primary production in the topographically complex CGOA are poorly known and difficult to quantify. Here we diagnose the output from a spatially nested, coupled hydrodynamic and lower trophic level model of the CGOA, to quantify both horizontal and vertical nutrient fluxes into the euphotic zone. Our nested model includes both nitrogen and iron limitation of phytoplankton production, and is driven by a fine-scale atmospheric model that resolves the effects of local orography on the coastal winds. Results indicate significant "rivers" of cross-shelf nitrogen flux due to horizontal advection, as well as "fountains" of vertical transport over shallow banks due to tidal mixing. Using these results, we constructed a provisional budget of nutrient transport among subregions of the CGOA. Contrary to expectations, this budget reveals substantial *upwelling* of nutrients over major portions of the shelf, driven by local wind-stress curl. These effects are large enough to overwhelm the smaller downwelling flux at the coast throughout the growing season. Vertical mixing by winds and tides, and horizontal flux from the deep basin, are other substantial contributors to nutrients above the 15-m horizon. These findings help to explain the productivity of this coastal ecosystem.

© 2009 Elsevier Ltd. All rights reserved.

1. Introduction

The Coastal Gulf of Alaska (CGOA) is a very productive area, supporting huge stocks of fish, birds, and other macrofauna (OCSEAP Staff, 1987; Sambrotto and Lorenzen, 1987). While such production is not unusual for coastal areas, it is more typically associated with areas where persistent upwelling-favorable winds bring nutrients to the surface. Conversely, the winds off of Alaska are generally downwelling-favorable at the coast over most of the year (Royer, 1998; Stabeno et al., 2004). Why, then, is this area so productive? Several alternative sources of nutrients have been suggested (Ladd et al., 2005a; Stabeno et al., 2004; Weingartner et al., 2002). These include: (1) "traditional" coastal upwelling in the summer, when winds are episodically upwelling-favorable; (2) Upwelling driven by wind-stress curl; (3) onshore flux of high-nitrogen low-chlorophyll surface waters from the deep basin; (4) onshore flux through canyons; and (5) vertical mixing on the shelf (e.g., driven by tides), with replenishment of the deep nutrient pool each winter.

Here, our intent is to quantify the various source pathways for nitrogen that fuels new production on the shelf. A more accurate accounting of these terms can ultimately help us to identify any bottom-up controls on the ecosystem operating on interannual to interdecadal time scales, a major focus of GLOBEC research (Weingartner et al., 2002). For such accounting we employ the Regional Ocean Modeling System described in Dobbins et al. (2009), coupled with the Gulf of Alaska NPZ model (henceforth termed the "GOANPZ" model) described in Hinckley et al. (2009). Where possible we compare these results with mooring and hydrographic data.

We begin with an overview of the region. The typical circulation patterns of the Gulf of Alaska are illustrated in Fig. 1. These include the Alaska Current/Alaskan Stream system located at the shelf break, as well as the Alaska Coastal Current (ACC) located at the coastline. The ACC is driven by the typically downwelling-favorable coastal winds and coastal runoff of the CGOA (Royer, 1998). Eddies with a mean diameter of 30 km are frequently associated with the ACC (Bograd et al., 1994; Hermann

---

* Corresponding author.
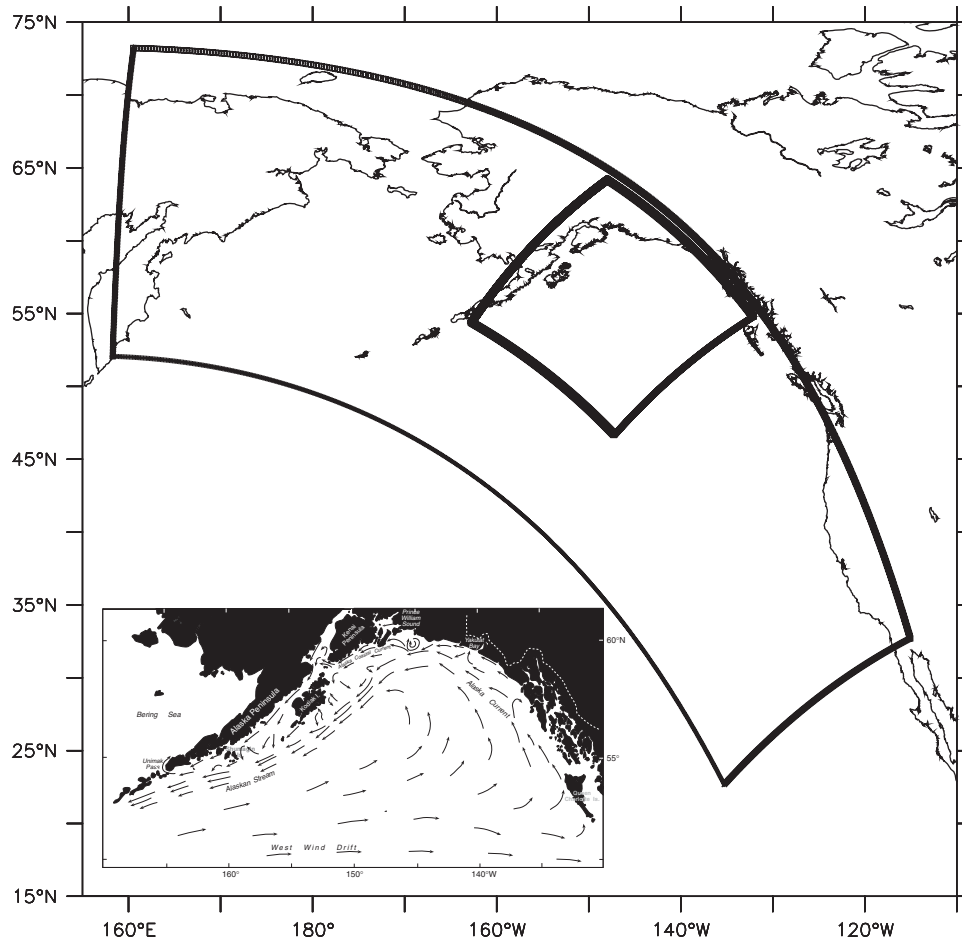*E-mail address:* Albert.J.Hermann@noaa.gov (A.J. Hermann).

Fig. 1. Diagram of the nested model grids. The two grids of interest are NEP (large box, 10 km), and CGOA (small box, 3 km). Inset is map of the Coastal Gulf of Alaska with its major current systems.

and Stabeno, 1996; Stabeno and Hermann, 1996; Williams, 2003; Williams et al., 2007). Shelf bathymetry includes a variety of submarine canyons, and an irregular coastline with many small coastal inlets. Eddies with a mean diameter of 200 km are frequently observed near the shelf break, and can have lifetimes of up to 2 years (Childers et al., 2005; Ladd et al., 2005b; Okkonen et al., 2003; Stabeno et al., 2004). These features of the shelf are discussed in more detail by Dobbins et al. (2009).

Average chlorophyll values derived from SeaWiFS data for the CGOA have revealed a strong cross-shelf gradient (Brickley and Thomas, 2003). A close-up view of mean July chlorophyll from SeaWiFS (Fig. 2) illustrates high values on the shelf, and especially high mean values around the rim of (but not necessarily in the center of) submarine banks near Kodiak Island. Cross-shelf transects of salinity, temperature, and nitrate at the Seward line (Nancy Kachel, pers. commun.) (Fig. 3) illustrate a core of less saline water near the coast associated with the ACC. In May 2001, reduced (but nonzero; generally 4–8 μmol kg^{-3}) values of nitrate are associated with this core, with relatively high concentrations across the seaward portion of the line. In September 2001, the freshwater core is intensified, and lower nitrate content is observed all across the shelf.

2. Methods

Our basic approach was to use a lower trophic level (NPZ) model embedded in a 3D circulation model driven by a mesoscale atmospheric model, to analyze nutrient fluxes on the CGOA shelf.

Here we offer a broad description of these models and some of the data used for model verification; for further details, the reader is referred to Dobbins et al. (2009) and Hinckley et al. (2009).

2.1. Circulation and NPZ models

The 3-D circulation model is based on the Regional Ocean Modeling System (ROMS). ROMS solves the primitive equations on a curvilinear-orthogonal horizontal grid and stretched vertical sigma coordinates (here with 30 levels). The mean horizontal spacing for the CGOA circulation model is ~3 km. This spacing resolves many of the significant mesoscale features of the region, including the prominent, 200-km-scale eddies at the shelf break (Ladd et al., 2005b). Vertical mixing is controlled by the KPP algorithm (Large et al., 1994). Boundary conditions for the physical model are set using spatial nesting with larger scale, coarser-grid implementations of ROMS (Curchitser et al., 2005; Hermann et al., 2009) (Fig. 1). Locally, winds and surface buoyancy flux are derived from atmospheric downscaling of NCEP hindcasts through the mesoscale model MM5, as described in Dobbins et al. (2009). General features of the wind field are revealed by monthly averages of wind stress and its curl in May and August 2001 (Fig. 4). The values shown are derived from atmospheric downscaling with the MM5 model. In both May and August, wind stress was downwelling-favorable at the coast (that is, tending to push surface waters towards the coast), with positive curl due to reduced wind-stress offshore.
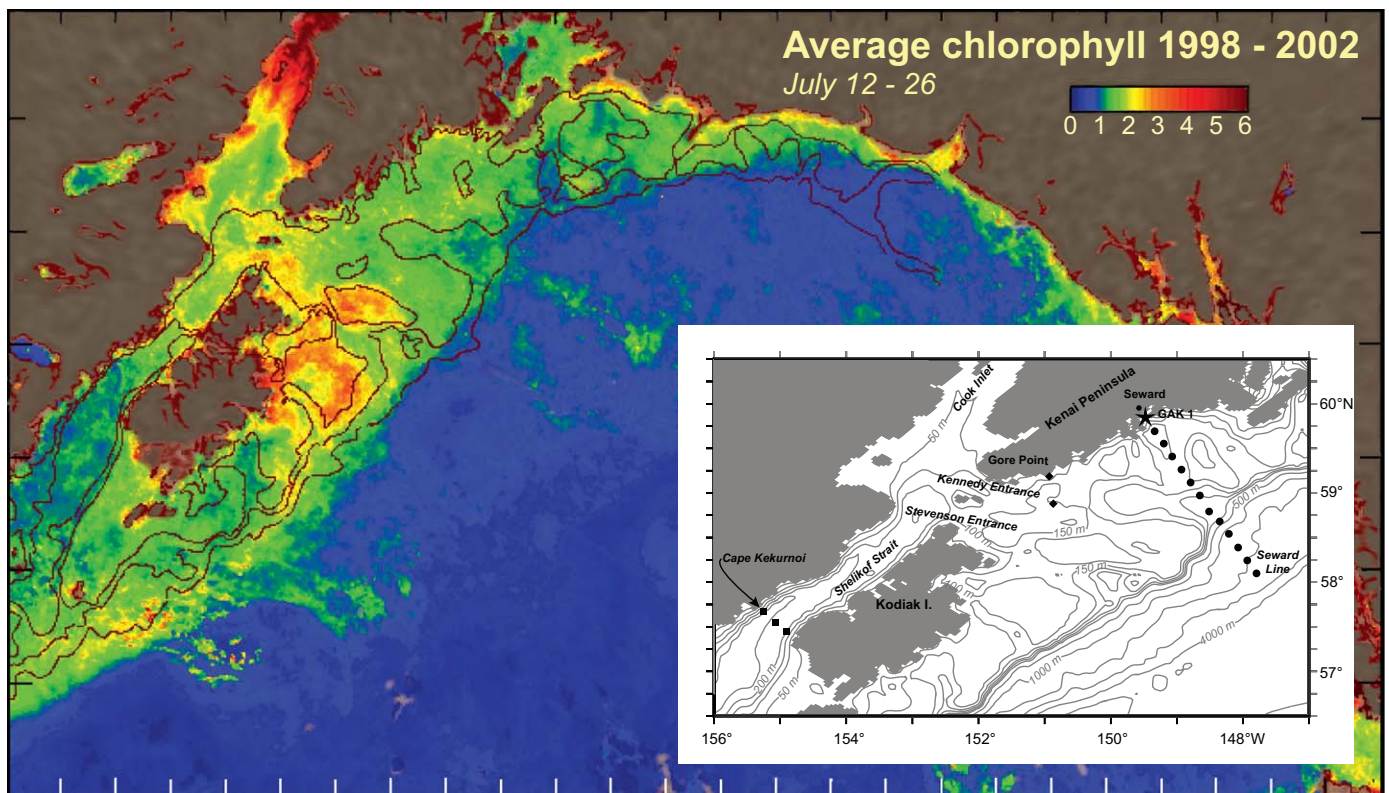
Fig. 2. Average surface chlorophyll from SeaWiFS data in the CGOA for late July, 1998–2002 (prepared by S. Salo, PMEL/NOAA). Values near coastlines are less reliable, due to contamination of the color signal by sediment. Inset shows bathymetry detail with location of the hydrographic and nutrient observations of Figs. 3 and 7 (Seward Line), and the current meter lines referred to in text (Gore Point, Cape Kekurnoi).

A distributed source of runoff is applied at the coastal boundary (as described by Dobbins et al., 2009), to replicate the many rivulets and streams of the CGOA. In the version of ROMS used here, freshwater was distributed vertically with a linear ramp, such that input was greatest at the surface. This vertical structure is intended to replicate some of the missing estuarine physics of this 3-km model. Four diurnal (O1, Q1, P1, and K1) and four semidiurnal (N2, S2, K2, and M2) tidal constituents are applied at the boundaries. The model was implemented on the massively parallel, distributed memory Linux cluster of NOAA's Forecast Systems Laboratory.

The CGOA physical model was run for the period December 2000–2002. Initial and lateral boundary conditions were derived from the larger Northeast Pacific (NEP) domain model (see Hermann et al., 2009). The NPZ model was run for the period 1 March–13 September 2001, and we focus on this time period because it corresponds with times of intensive GLOBEC sampling in the CGOA. For the purposes of this study, 2001 can be considered a typical year. Although the period of April–September 2001 included slightly lower than normal sea-level pressures in the central GOA, wind anomalies on the shelf south of the Kenai Peninsula near 59°N, 150°W, as estimated with the NCEP Reanalysis and an empirical correction for the effects of the coastal orography (Stabeno et al., 2004), were only about $1 \, \mathrm{m \, s^{-1}}$ in the cross-shelf component (directed offshore) and near zero in the alongshelf component.

The NPZ model used for this CGOA study (GOANPZ) is described in Hinckley et al. (2009). This model includes multiple size classes for phytoplankton and microzooplankton, as well as larger mesozooplankton (e.g., neritic copepods and oceanic copepods) (Fig. 5). Limiting macronutrients were nitrate and ammonium. One significant aspect of the GOANPZ model is the inclusion of iron as a limiting micronutrient. For this purpose, the model uses an iron regulation scheme similar to that of Fennel

et al. (2003), which includes a Michaelis–Menten response of maximum photosynthetic rate to iron-deficiency, with photosynthetic efficiency increasing proportionally to the iron concentration and a saturation region. Iron is not followed throughout the entire ecosystem model; instead, iron levels are decreased by small and large phytoplankton uptake, and then nudged back to climatological values, with a nudging factor of $0.033 \, \mathrm{d^{-1}}$. Iron climatology is set to $2.0 \, \mu \mathrm{mol \, m^{-3}}$ everywhere on the shelf, and 0.05 (surface)–0.6 (deep) $\mu \mathrm{mol \, m^{-3}}$ offshore, based on data collected by the VERTEX program (Martin et al., 1989). With the addition of iron as a limiting micronutrient and multiple size classes of plankton, the model captures the observed structure and seasonality of cross-shelf and vertical gradients of nitrogen and chlorophyll (Hinckley et al., 2009; Coyle et al., in prep.). The GOANPZ model is embedded in the circulation model, and so experiences the same instantaneous velocities and mixing as the physical model, including tides. All output was lowpass filtered with a 40-h Cosine-Lanczos filter to remove tidal and other subinertial signals, and stored as daily values; these daily values were used for calculating the fluxes.

As described in Hinckley et al. (2009), initial and boundary conditions for the biological variables were estimated using vertical profiles of observational data collected by the GLOBEC-NEP Long-Term Observation Program on the Seward Line (http://www.ims.uaf.edu/GLOBEC/). At the coast, the freshwater source is prescribed with $2 \, \mu \mathrm{mol \, kg^{-3}}$ of nitrate and $2 \, \mu \mathrm{mol \, kg^{-3}}$ of iron.

2.2. Circulation, hydrographic, and nutrient data

For circulation model-data comparison, we will illustrate average summertime horizontal velocities, as in Dobbins et al. (2009). Maps of horizontal velocity were derived from
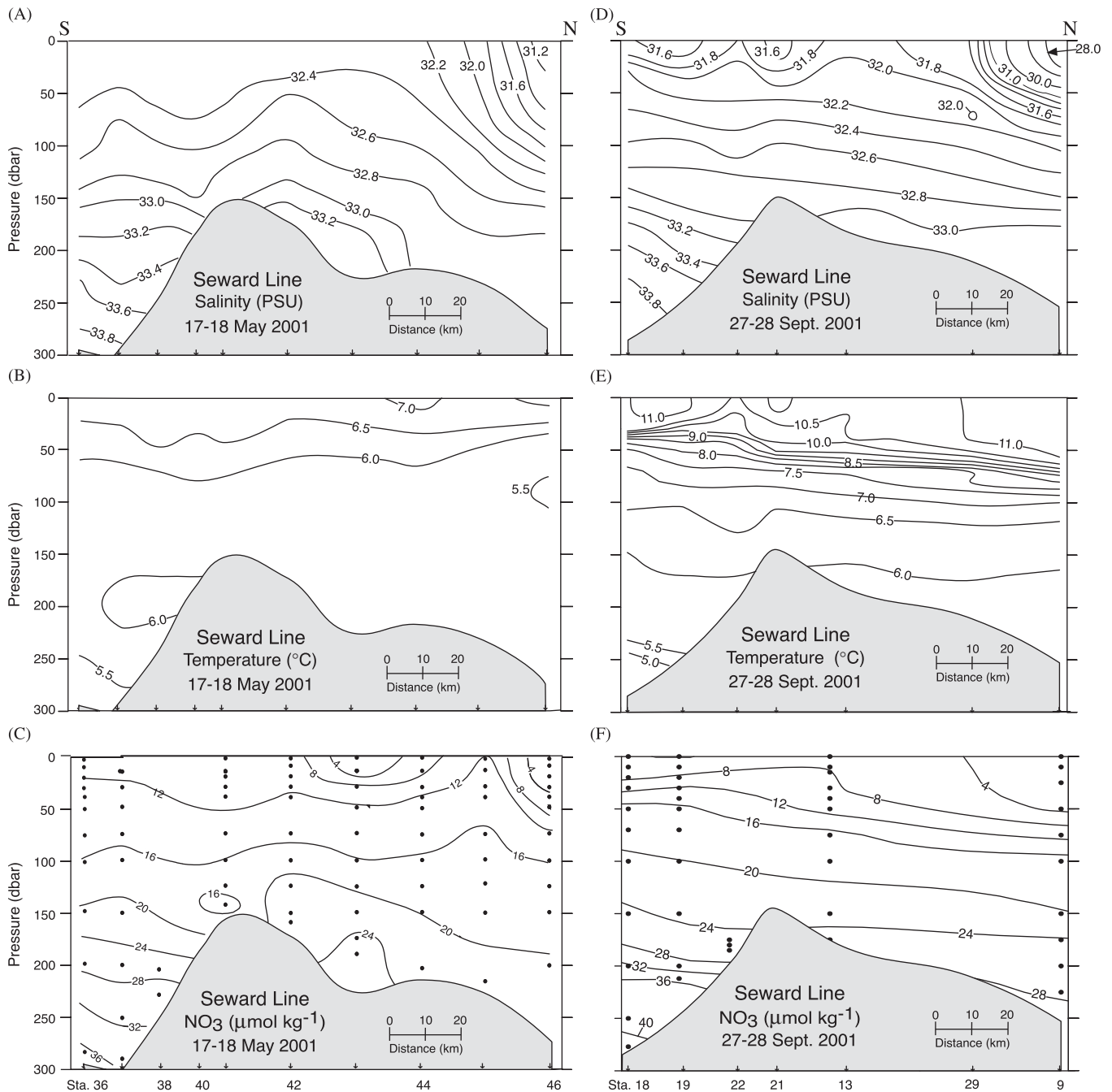
Fig. 3. Spring and late summer salinity, temperature and nitrate transects along the Seward Line (see Fig. 2) from hydrographic surveys. Left panel is May 2001; right panel is September 2001. The Alaska coast is to the right in these panels.

approximately 10 years of data from satellite-tracked drifters drogued at ~40 m (Stabeno et al., 2004). All available velocity estimates within 0.5° longitude by 0.25° latitude bins were averaged for summer (here defined as May–September). Only bins that had at least four independent velocity estimates were included in the map; independence is here defined as being separated by at least 3 days (which is the dominant decorrelation time for subtidal velocities in this region). Observations from waters deeper than 3000 m were excluded, as these are improperly aliased by large, persistent 200-km-scale eddies. Equivalent model velocities on the same grid were obtained by temporally averaging over the same summer period for

2001–2002. Additionally, we use observations along the Seward Line (see Fig. 2) from cruises during May and September 2001, for comparison with the daily model output. These data are from transects undertaken on the R/V *Ron Brown* (in May) and the NOAA ship *Miller Freeman* (in September). Conductivity–temperature–depth (CTD) casts were taken with a Seabird SBE-911 Plus system. Salinity calibration samples were taken on all casts and analyzed on a laboratory salinometer. Water samples for nitrate and other inorganic nutrients were collected using 5-L Niskin bottles. Samples were syringe-filtered using 0.45-μm cellulose acetate membranes, and the filtrate was collected in 30-mL acid-washed high-density polyethylene bottles after three rinses.
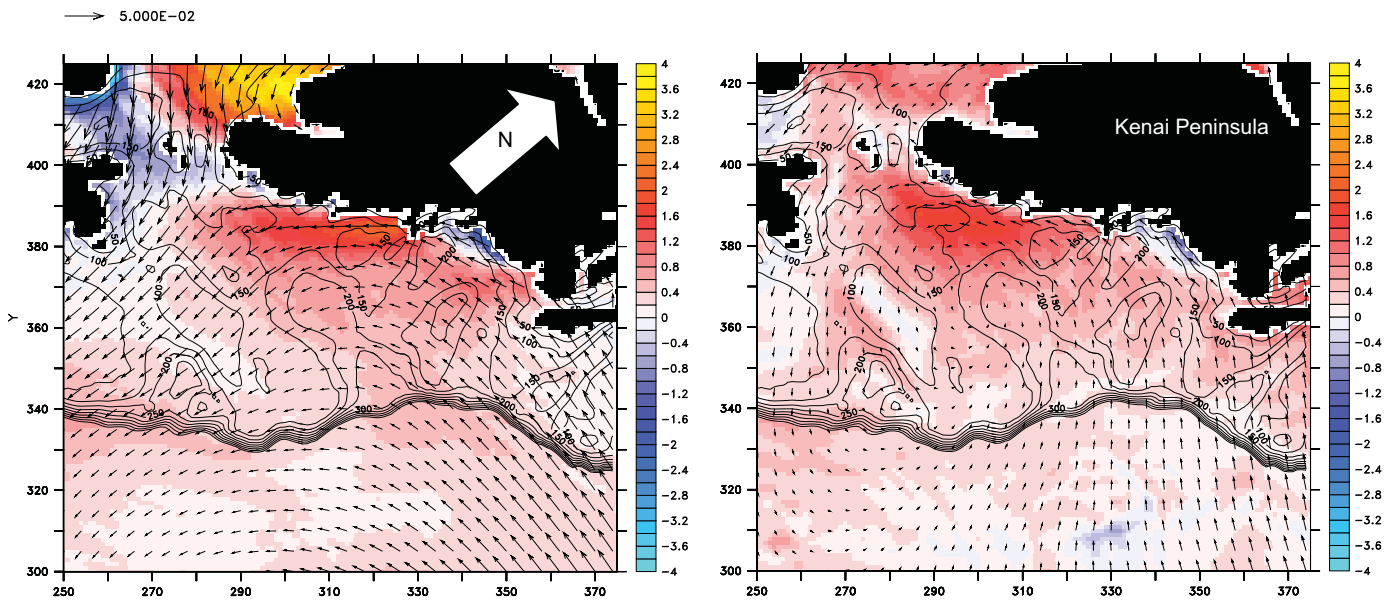
Fig. 4. Monthly average wind-stress vectors (N m^{-2}) and wind-stress curl (N m^{-3} × 10^3, shaded) calculated by the models for May 2001 (left panel) and August 2001 (right panel). In these figures, the x- and y-axis are in native model coordinates with grid spacing ~3 km. Locations of Amatouli Trough and Albatross and Portlock Banks are indicated.
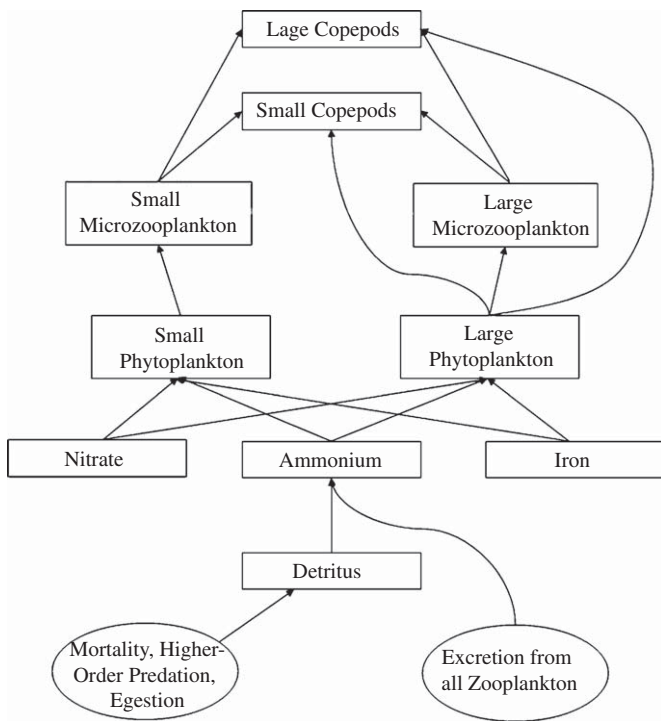

Fig. 5. Structure of the GOANPZ ecosystem model used in this study (from Hinckley et al., 2009). Arrows indicate the direction of material flux.

Samples were frozen at −20 °C with care to leave appropriate head space and to freeze upright (Dore et al., 1996). Samples were analyzed at PMEL within 12 months. Samples were thawed in a cool water bath and immediately analyzed. Nitrate concentrations were determined using components from Alpkem and Perstorp instrumentation. Analytical methods were from Armstrong et al. (1967) and Atlas et al. (1971). Standardization and analysis procedures specified by Gordon et al. (1993) were closely followed, including calibration of labware, preparation of primary and secondary standards, and corrections for blanks and refractive

index. Nitrate values were accurate to <2% full scale (<1 μM nitrate).

2.3. Nutrient flux calculations

Physical sources for any scalar property in this system include horizontal advection, vertical advection, and vertical diffusion:

$$C_t = -uC_x - vC_y - wC_z + (kC_z)_z + B \tag{1}$$

where C is the scalar property, u,v,w are velocities in the x,y,z directions, respectively, k is the vertical diffusivity, and the subscripts denote partial differentiation. In the case of nitrate, the non-conservative term B consists of uptake by phytoplankton (i.e., "new production"). For our study, we consider a control volume of 15 m depth, which spans the shelf out to the 500 m isobath (~200 km offshore), and spans approximately 300 km alongshelf, from Prince William Sound to the entrance of Shelikof Strait (Fig. 8). We will refer to this as the "0–15 m" control volume, but in our calculations (as in the real ocean) the upper boundary in fact corresponds to the sea surface, and hence is not precisely $z = 0$ on any given day. We calculate the fluxes into and out of this control volume across each face of the box. This construction is equivalent to a volume integral (from 15 m below mean sea level, up to the sea surface) of the local balance of terms:

$$\begin{aligned} C\_box_t &= \iiint [-uC_x - vC_y - wC_z + (kC_z)_z + B]\, dx\, dy\, dz \\ &= C\_east + C\_west + C\_north + C\_south \\ &\quad + C\_vertadv + C\_vertdiffu + B\_box \end{aligned} \tag{2}$$

Here the directions north, south, east and west are relative to the orientation of the model grid, which is actually southeast-to-northwest in our area of interest (see Fig. 6 for orientation). All of these terms have been defined as positive/negative for fluxes into/out of the control volume. The terms C_vertadv and C_vertdiffu represent upward flux across the 15 m depth horizon due to upwelling and vertical diffusion, respectively.

It is important to note that the relative strength of horizontal and vertical terms entering this control volume is highly dependent on the dimensions of the box. A control volume of
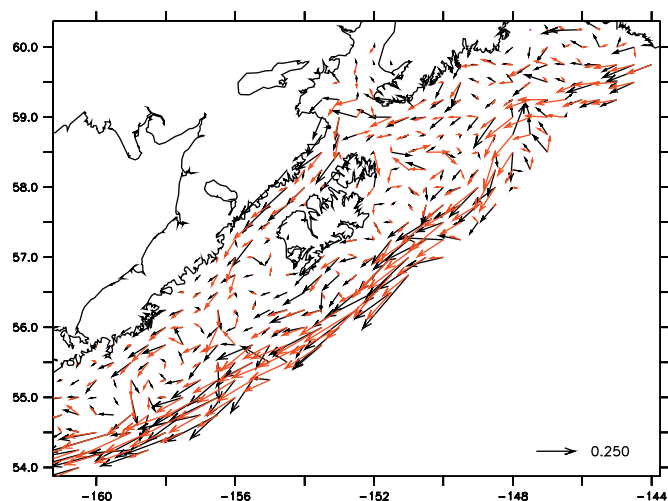
Fig. 6. Mean velocity vectors (ms^{-1}) at 40 m on the CGOA shelf for May–September, computed from drifter data (black) and model output (red).

large horizontal extent typically will not be strongly affected by horizontal fluxes, as compared to vertical ones. For a narrower box, horizontal inflows and outflows will typically be larger relative to vertical flows, but note that the sum of horizontal fluxes may still be inconsequential if no horizontal gradients of velocity or tracer are present.

To highlight flux terms for the shelf alone, we include in our 0–15 m control volume only those horizontal areas of the CGOA where the bathymetry is shallower than 500 m. Defined in this way, the C_south term is in fact the flux from the deep basin to the shallower shelf in the top 15 m of the water column, and the C_vertadv and C_verdiffu terms represent paths by which deeper fluxes from the basin onto the shelf (or deeper fluxes from upstream on the shelf) may enter the control volume. The total horizontal area of the control volume is $\sim 6 \times 10^{10}$ m^2.

We focus here on fluxes of nitrate into/out of the control volume (0–15 m depth). Nitrate is a limiting nutrient for phytoplankton growth on the inner and middle CGOA shelf in summer (Strom et al., 2006), and its uptake represents new production to the ecosystem. The 15-m depth horizon was chosen as a crude representation of the "euphotic zone", where light levels are high enough to drive net production. We concede that this choice is somewhat arbitrary, as sediment levels, self-shading, and incident PAR at the sea surface will cause the euphotic depth to vary both spatially and seasonally.

An alternate way to analyze the fluxes would be to map the advective and diffusive terms at each gridpoint. The virtue of the control volume approach is to integrate these terms over a broad spatial area, so as to summarize the macronutrient characteristics of the shelf community (or communities) as a whole. However, fluxes through the 15-m depth horizon were also examined for spatial patterns ("hot spots") of advection and mixing across that surface.

The flux terms in Eq. (2) were calculated using stored daily averages of u, v, w, k, and nitrate from the CGOA circulation and GOANPZ models, interpolated to constant depth levels. Daily averages of free surface height were employed when calculating the integrals. It is recognized that this procedure may exclude some flux due to the interaction of tides with time-variable gradients; however, because our runs used daily average forcing, the nutrient gradients had little variance on hourly scales, hence this bias should be negligible. In the plots shown here, time series were smoothed with a 30-day running average to emphasize the seasonal evolution of properties.

3. Results

3.1. Model-data comparisons

A comparison of atmospheric (MM5) and oceanic (CGOA) circulation model results with data is presented in Dobbins et al. (2009), and includes the following elements: (1) winds and shortwave radiation at a mid-shelf location; (2) hydrography along cross-shelf lines; (2) total flux and potential energy anomaly (a summary statistic of stratification) through Shelikof Strait; (3) horizontal maps of mean summer and winter velocities over the shelf; (4) vertical sections of velocities (means and EOFs) at Gore Point. Statistically significant (at the 1% level) correlations between model and data were demonstrated with the following R^2 values: mid-shelf winds (0.58); mid-shelf shortwave radiation in the summer (0.38) and winter (0.74); total flux through Shelikof Strait in summer (0.39) and winter (0.59); mean E/W velocities at 40 m depth (0.54); mean N/S velocities at 40 m depth (0.38); and the amplitude time series for the dominant EOF patterns of alongshore velocity derived from a cross-shelf/depth section at Gore Point (0.37).

For the hydrodynamic run used in our study, we illustrate model-data correspondence of mean summer velocities, where the observations are derived from drifters as described earlier (Fig. 6). The modeled spatial means of N/S and E/W currents are each within ~ 2 cm s^{-1} of their observed values, and the R^2 of these properties with their measured equivalents are 0.51 and 0.36, respectively (both significant at the 1% level). The model replicates the mean pattern of the ACC and Alaskan Stream, as well as clockwise gyres above the shallow banks southeast of Kodiak Island (e.g., Portlock Bank).

A description of the GOANPZ model and its correspondence to data is more fully explored in Hinckley et al. (2009) and Coyle et al. (in prep.). In each of these studies, it is demonstrated that the model (with iron as limiting micronutrient) captures the observed cross-shelf and vertical gradients of nitrogen and chlorophyll. Here, we compare measurements along the Seward Line (Fig. 3) with their model equivalent (Fig. 7). Shown are the daily fields for salt, temperature, and nitrate from the model, sampled along the same cross-shelf section as the data. The final time step of the GOANPZ model run (13 September) is shown for comparison with the fall data, which was measured 2 weeks later in the season. Basic observed features replicated by the model include: (1) strongly stratified waters near the coast, with expansion of the freshwater out onto the shelf in the fall; (2) weak temperature gradients in the spring, with a strong thermocline in the fall, (3) surface depletion of nitrate to 0–4 µmol kg^{-3} values near the coast, with expansion of the depleted area over the shelf in the fall; (4) nitrate values > 16 µmol kg^{-3} below 100 m depth in both seasons.

3.2. Mass balance of water

Before calculating nutrient fluxes for the control volume, it is worthwhile examining the flux of water itself. Fig. 8 illustrates a high degree of mesoscale structure to the vertical velocity field in early spring (other times exhibit similar mesoscale structures). In particular, traditional two-dimensional downwelling along the Alaskan coastline is rare. More typically, patterns with alternating upwelling and downwelling cells prevail. When we sum the advective terms over the control volume (Fig. 9), we find advection from the east (C_east), plus advection in from the basin (C_south), being nearly balanced by advection out to the west (C_west). However, we find that water is advected upward (that is, upwelling) across the 15-m depth horizon in March and
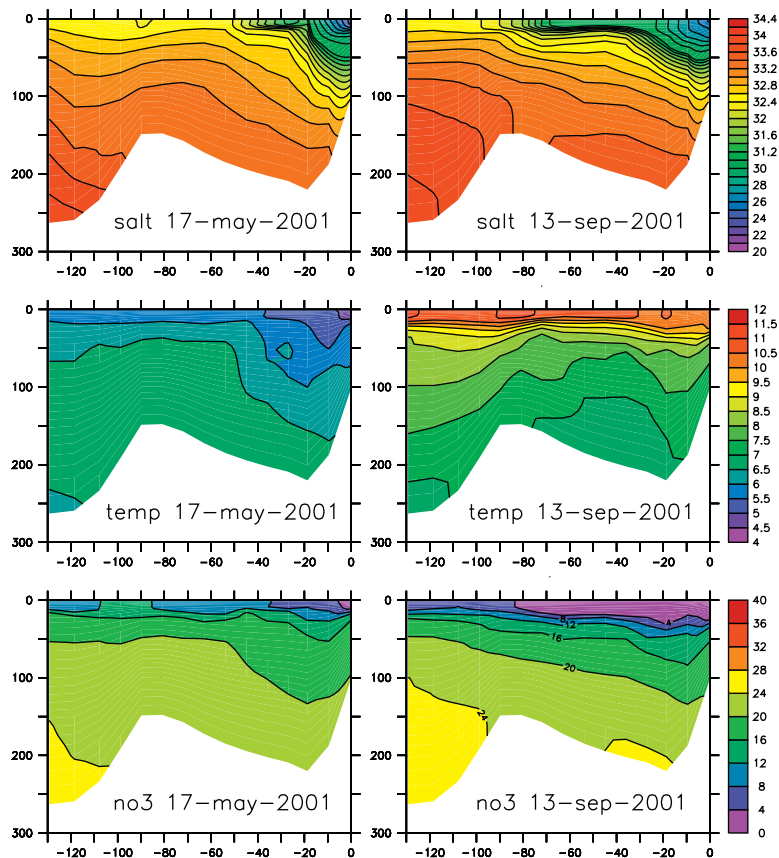
Fig. 7. Salinity, temperature (°C) and nitrate (millimole m^{-3}) transects along the Seward Line (see Fig. 2) from the hydrodynamic and NPZ models. Panels on left are May 2001; panels on right are September 2001. The Alaska coast is to the right in these figures. The x-axis shows distance offshore (km) and the y-axis is depth (m).

April of 2001, with smaller episodes in July and August. Conversely, water is downwelled in May and June of that year. This is unexpected in light of the downwelling-favorable coastal winds observed over most of the year in the CGOA. Apparently, the seasonal pattern of upwelling–downwelling in the control volume reflects the shelf-wide wind-stress curl, rather than a coastal wind-stress per se. These results are consistent with the wind-stress curl patterns revealed in Fig. 4. Integrated over the control volume, the monthly means of wind-stress curl, converted to equivalent Ekman flux, are correlated with the model's 15 m upwelling ($R^2 = 0.80$, significant at the 1% level) (Fig. 10).

3.3. Spatial patterns of nitrate flux within the control volume

A snapshot of surface nitrate from the model is shown in Fig. 11 for 1 May 2001. The model replicates the low-nitrate values close to the coast, and the higher values further out. The Alaskan Stream and the Alaska Coastal Current are both evident in the surface current vectors, as well as 30-km-scale meanders in the Alaska Coastal Current. By multiplying current vectors times nitrate values at 15 m depth, we obtain a map of horizontal nitrate flux (Fig. 12). This reveals intense "rivers" of nitrate along the shelf break and near the coast in spring. It also indicates anticyclonic circulation of nitrate around Portlock Bank. Daily flux maps (not shown) suggest intermittent onshelf penetration of nitrate along the northern bank of Amatouli Trough, but this does not appear significant in the monthly average. By multiplying the vertical velocities at 15 m depth times the local nitrate values, we obtain a map for vertical flux of nitrate across the bottom of the control volume (Fig. 13). This field, like the vertical velocities themselves (Fig. 8), is quite patchy, with alternating cells of upwelling and

downwelling nutrients. To some degree these cells appear related to small-scale bathymetric features. This is expected insofar as cross-isobath flows (and a consequent rising and falling of water parcels) are associated with small-scale bathymetric features; frontal phenomena around the edges of larger scale bathymetric features also contribute to vertical motions. Calculated vertical diffusion (Fig. 13) indicates the expected source term in most areas, with intense "fountains" of vertically diffused nutrients over Portlock Bank and Albatross Banks, and downstream of Kennedy Entrance/Cape Elizabeth. A plot of surface velocity and nitrate for 15 August 2001 (Fig. 11) reveals depleted stocks of nitrate. Substantial onshelf and alongshelf flows of nitrate, so evident in May, are now absent (Fig. 12). Some anticyclonic nitrate flux around Portlock Bank is still in evidence, but at reduced magnitude relative to May. Drifter and nutrient data (not shown) conform to this general picture around Portlock Bank, which suggests an upward/downward spiral of nutrients around the margin of the bank; these features will be a subject of a separate paper.

3.4. Flux summary for the control volume

We integrate the fluxes across the faces of the control volume, to generate simple time series of their amplitude during 2001 (Fig. 14). Monthly averages are summarized in Table 1. For the chosen control volume, vertical diffusion is the dominant term, with a maximum flux in early May. Advection of nitrate in from the east, and advection out to the west, are dominant terms in the early part of the growing season when nitrate levels are highest. Advection in from the basin also plays an important role, especially during mid-April–mid-June. Vertical advection of
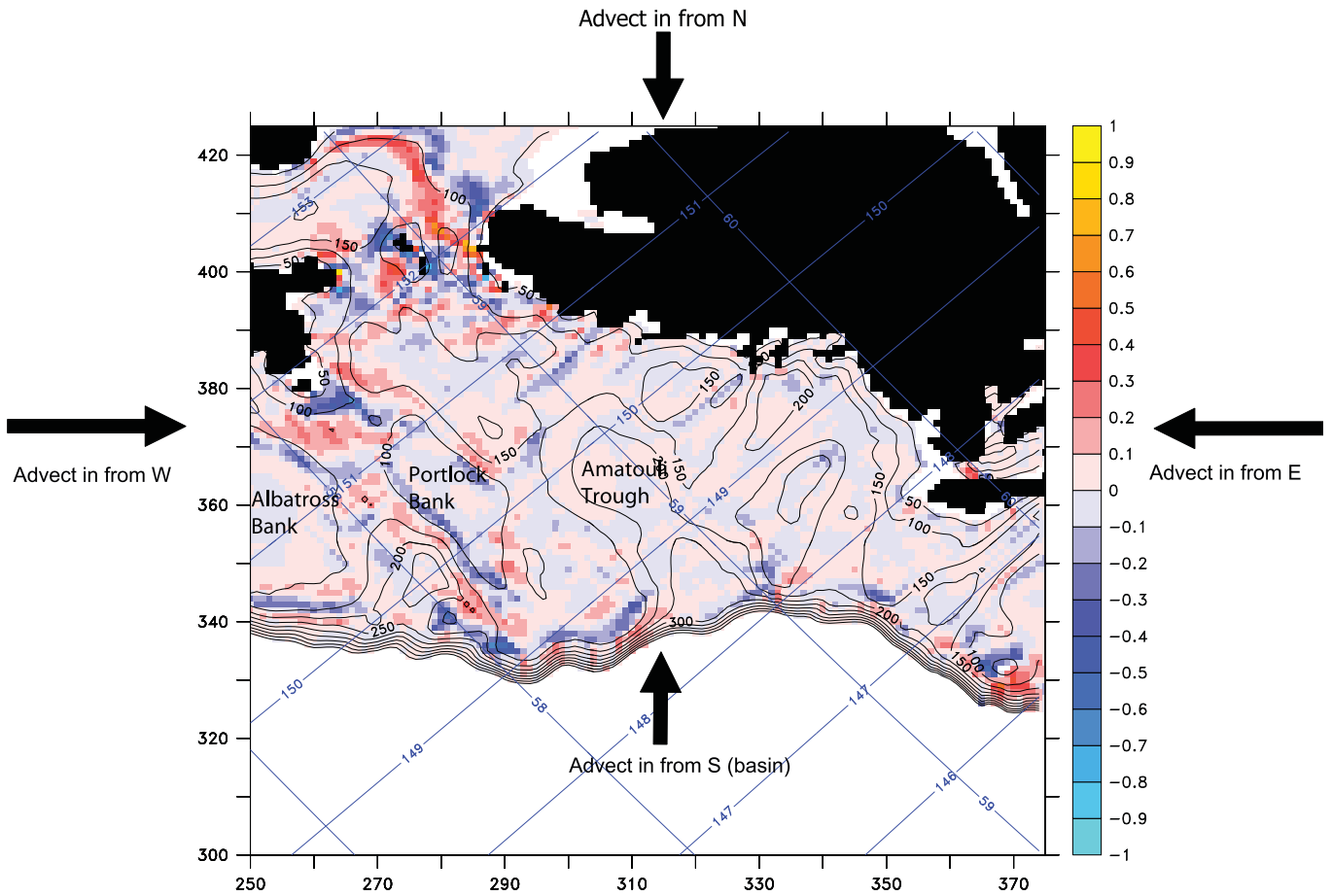
Fig. 8. Control volume used in water and nutrient flux calculations. Calculated monthly average vertical flux of water (mm s^{-1}) through the 15-m-depth horizon for May 2001 is shaded. Positive/negative values indicate upward/downward flux. In this and subsequent spatial maps, the *x*- and *y*-axis are in native model coordinates with grid spacing ~3 km. Also shown here are bathymetry (black lines) and the latitude–longitude grid (blue lines).
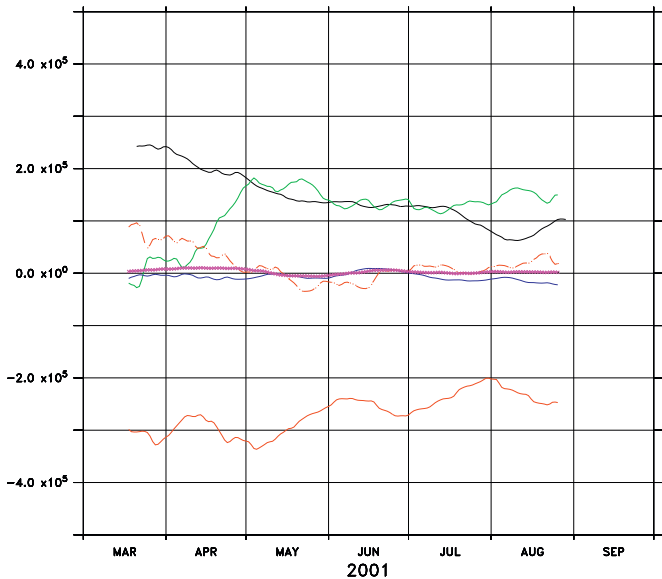

Fig. 9. Lowpass-filtered time series of water flux (m^3 s^{-1}) into the control volume. black = C_east, red = C_west, green = C_south, blue = C_north, dashed red = C_vertadv, magenta = sum of advective terms. Positive/negative values indicate flux into/out of the control volume.

Fig. 10. Time series of Ekman pumping from the wind-stress curl simulated by the MM5 (black line) and vertical velocities at 15 m from the CGOA/MM5 ROMS simulation (red line). These velocities are integrated over the control volume, which is an area of ~6 × 10^{10} m^2. Shown are daily values (solid) and their 30-day running mean (dashed). The units are m^3 s^{-1}.

nitrate (that is, upwelling of nitrate) is a substantial source term during March and April, and a slight loss term beyond early June, despite the net upwelling of water indicated for July–August in
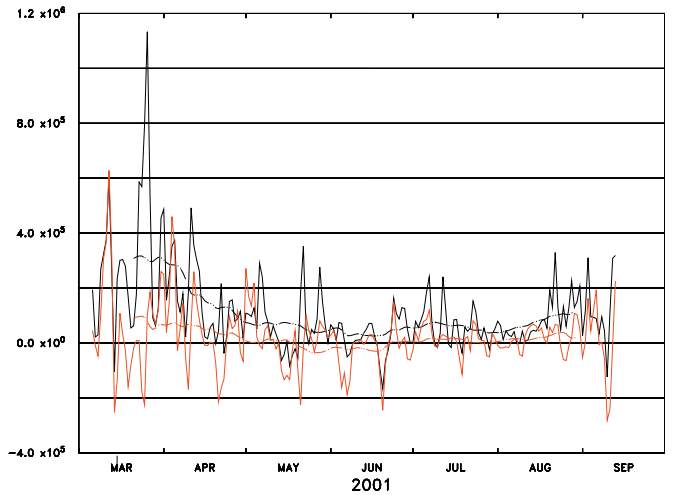
the water mass balance of Fig. 9. The sum of advective terms is slightly positive (that is, a net source of nitrate to the control volume) in March, April, and late May, and slightly negative (a net sink) after mid-June. The sum of vertical diffusion plus all advective terms is consistently positive, with a maximum in
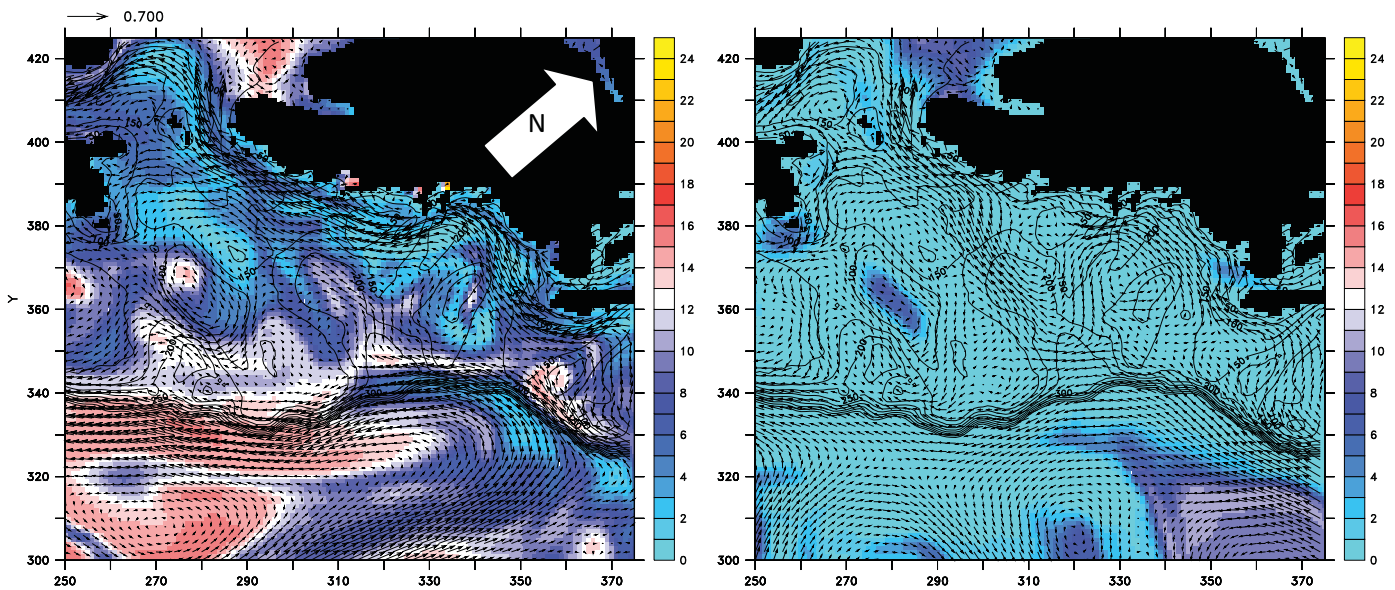
Fig. 11. Modeled surface nitrate (millimoles m^{-3}) and velocity (m s^{-1}) on 15 May 2001 (left panel) and 15 August 2001 (right panel).
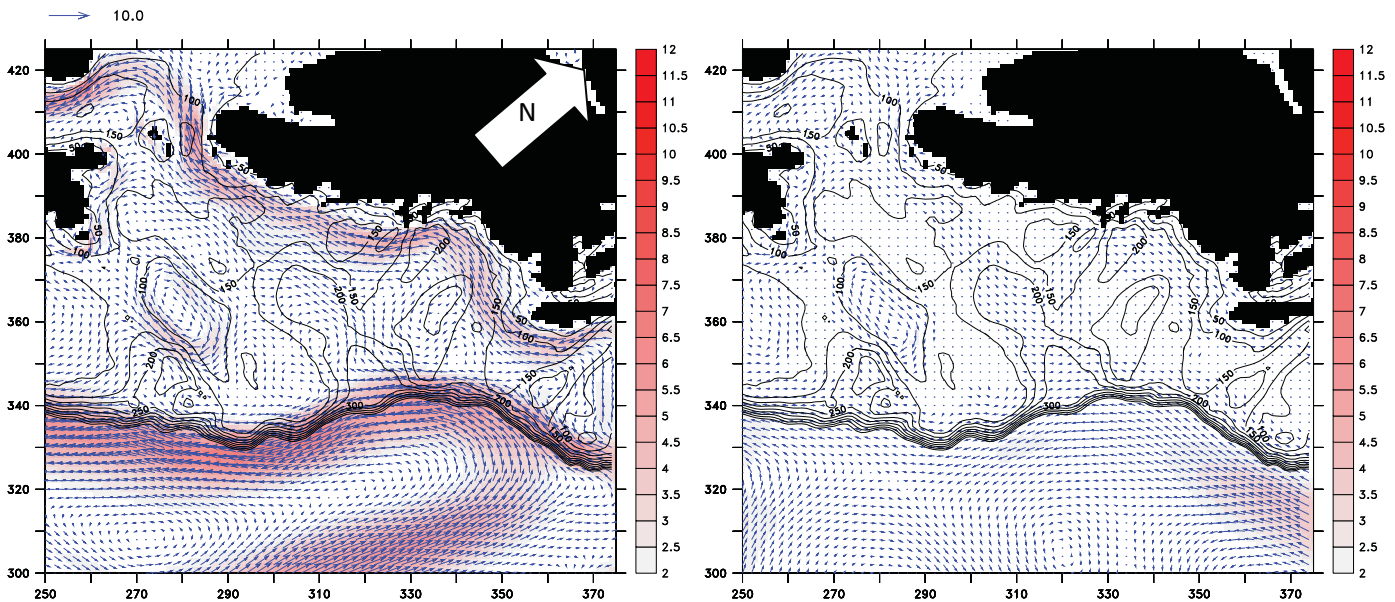

Fig. 12. Modeled monthly average horizontal flux of nitrate at 15 m depth (millimoles m^{-2} s^{-1}) for May 2001 (left panel) and August 2001 (right panel). The vectors represent magnitude and direction of nitrate flux, i.e., the velocity vector multiplied by the value of nitrate at that location.

May. This reflects the quantity of new production occurring in the control volume. Averaged over the entire time period shown, we obtain a value of 4.0 mmol nitrate m^{-2} d^{-1}, which is within the range of 2.46–6.97 mmol nitrate m^{-2} d^{-1} reported for this region by Childers et al. (2005).

3.5. Dependence of the mass balance on the control volume

When similar calculations are performed on a smaller control volume, some significant differences emerge. In Fig. 15, we map the horizontal and vertical advection of nitrate near Amatouli Trough, as well as the vertical diffusion of nitrate across the 15 m depth horizon. As with the larger control volume, we see rivers of horizontal nitrate flux, a patchy field of upwelling and downwelling, and a net source of nitrate due to vertical diffusion. When we sum these terms over the control volume (Fig. 16), we again find substantial horizontal advection in from

the east and out to the west. Due to the smaller horizontal extent of this control volume, vertical diffusion plays a less dominant role as compared to the horizontal advection terms. Here, its contribution is similar to that of advection in from the deep basin. Nonetheless, as for the larger control volume, vertical diffusion is larger than the sum of the advective terms at all times.

4. Discussion

4.1. Advection of nitrate from the deep basin

It has been suggested that the high productivity of the CGOA shelf results from the confluence of high-iron, low-nitrate waters on the shelf with high nitrate (or more specifically, high-nutrient low-cholorophyll), low iron waters from the basin (Stabeno et al., 2004). In our budget we have found advection of nitrate in from
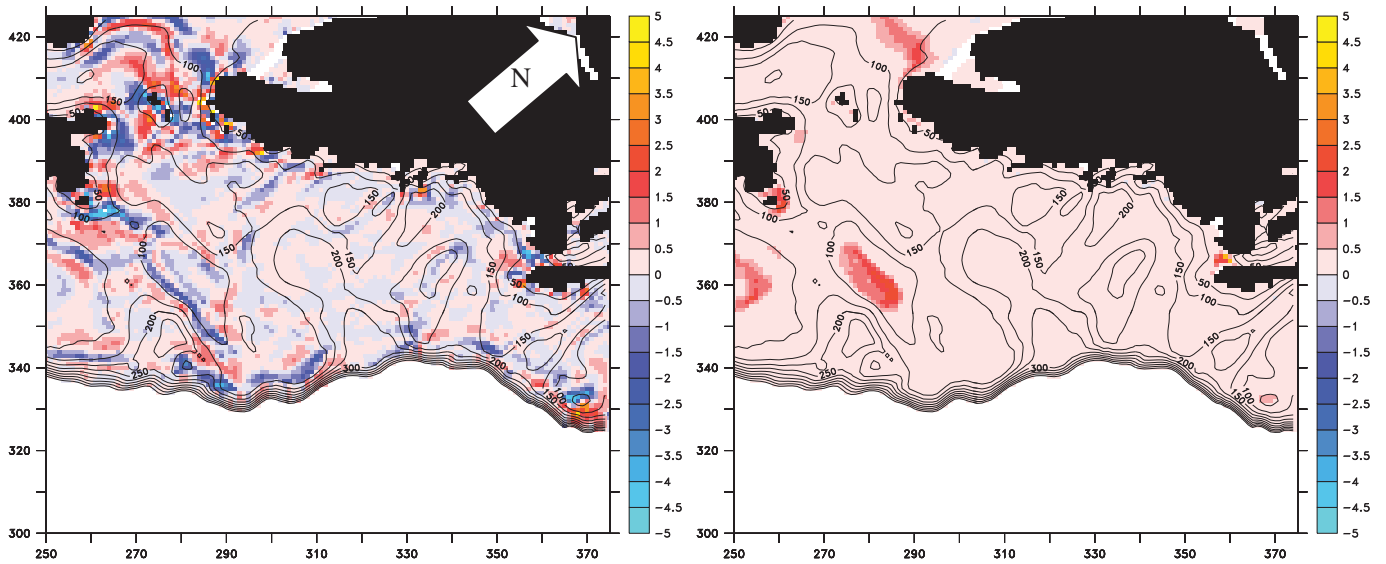
Fig. 13. Modeled monthly average vertical advection (left panel) and vertical diffusion (right panel) of nitrogen across the 15 m depth horizon (millimoles $m^{-2}\,s^{-1} \times 10^3$) for May 2001.
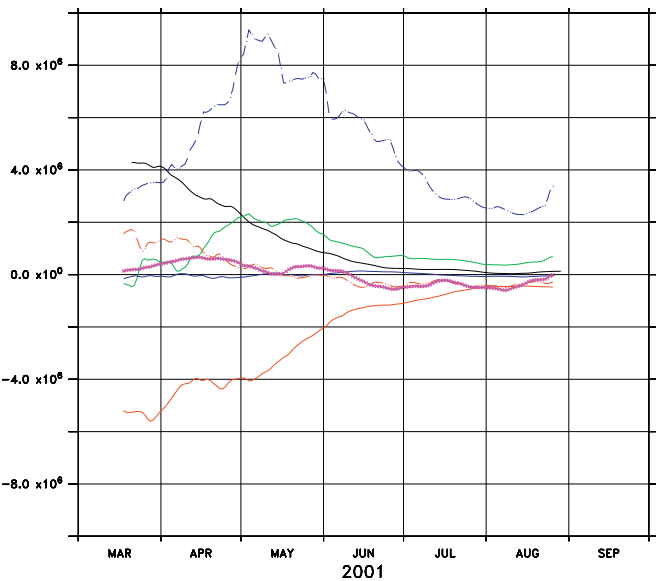

Fig. 14. Lowpass-filtered time series of nitrate flux (millimoles s^{-1}) into the control volume. red = C_west, black = C_east, green = C_south, blue = C_north, dashed red = C_vertadv, dashed blue = C_vertdiffu, magenta = sum of advective terms. Positive/negative values indicate flux into/out of the control volume.

Table 1
Monthly average fluxes of nitrate into the control volume for the advective and diffusive terms.

	A_east	A_west	A_south	A_north	A_below	D_below	Tot_A	Tot_A+D
March	42.82	−51.98	−3.34	−1.63	15.53	28.18	1.39	29.57
April	28.89	−40.45	10.02	−0.43	8.29	62.14	6.32	68.46
May	12.12	−31.63	20.44	−0.07	−0.35	73.28	0.52	73.80
June	3.71	−12.65	9.81	1.36	−4.80	59.12	−2.56	56.56
July	1.96	−7.74	5.83	−0.19	−2.06	28.97	−2.20	26.77
August	0.68	−4.36	4.33	−0.88	−3.51	22.93	−3.73	19.19

All values shown are millimole $s^{-1} \times 10^5$.

modeling study, Skogen et al. (1995) calculated advective throughflows of total nitrogen among various subareas of the North Sea; among these, the subarea containing the Norwegian Coastal Current exhibited the largest throughflow. While recent high-resolution biophysical modeling has been carried out for the Norwegian Coastal Current (e.g., Skogen et al., 2007), to our knowledge a full nitrogen budget (that is, a comparison of flux terms) has been not been calculated for this area. A different model-based nitrogen budget for the Dogger Bank region of the North Sea (Proctor et al., 2003), found that on annual timescales, vertical diffusive flux across the thermocline exceeded the horizontal throughflow above the thermocline. As noted in Section 2.3, such total flux budgets will be highly dependent on the dimensions of the box, as well as the fluxes through the boundaries; this is demonstrated in our comparison of the entire shelf budget (Fig. 14) vs. the Amatouli Trough budget (Fig. 16).

4.2. Nutrient fountains

It is noteworthy that upward vertical diffusion of nitrate in May is maximal around the margins of the Portlock and Albatross Banks, rather than at their centers. This conforms to the map of mean chlorophyll (albeit from later in the season) shown in Fig. 2. GLOBEC modeling work in the Gulf of Maine and Georges Bank area (Franks and Chen, 1996, 2001; Ji et al., 2006) is relevant to these results. As with Portlock Bank, tidally generated mixing occurs in the center and along the margins (flanks) of Georges
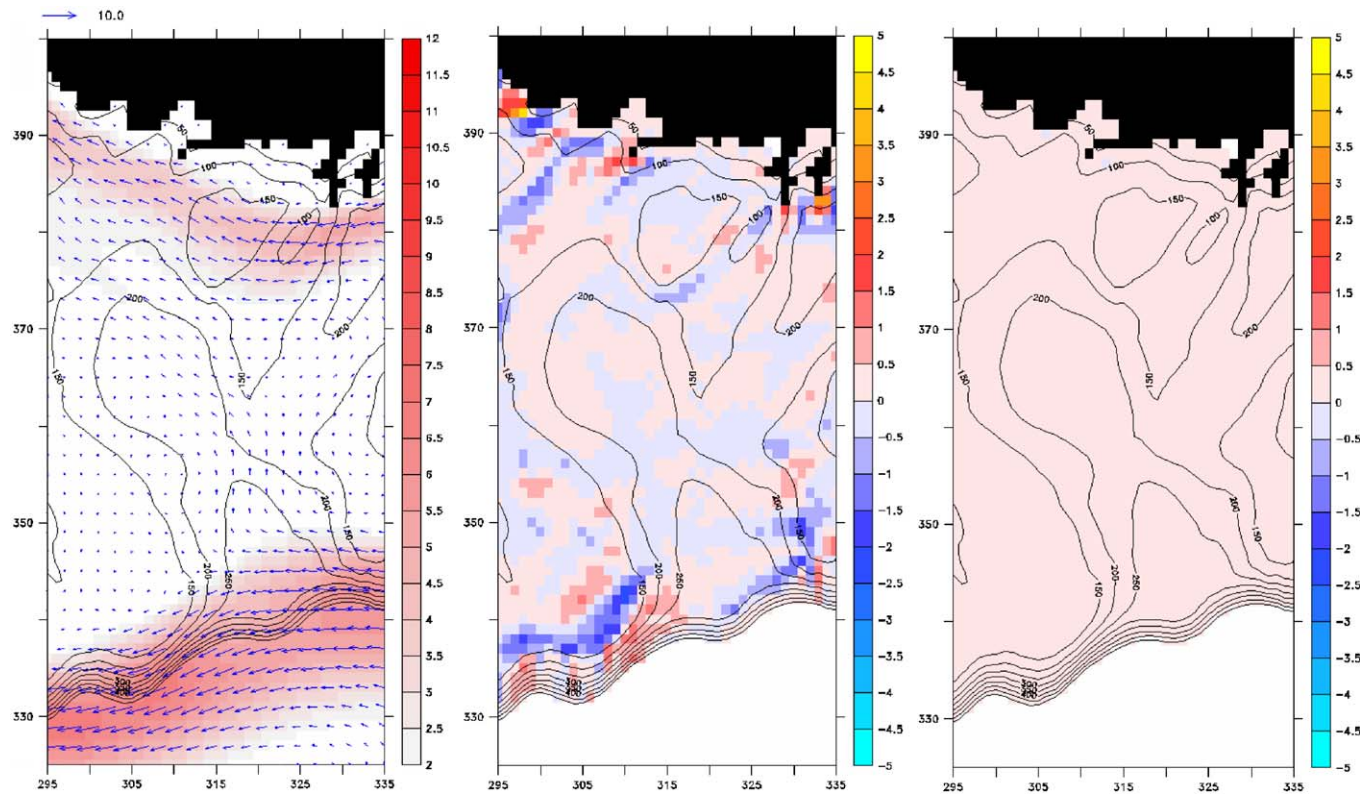
the deep basin above the 15-m depth horizon, all throughout the growing season. While not the largest term in the nutrient budget for either of our control volumes, this source of nitrate is substantial, and likely contributes to the high values of primary production observed for the shelf. The dominance of the vertical diffusion term in these budgets underscores the need for NPZ models which encompass the entire year, and nutrient budgets for deeper depth strata. With these, it would be possible to quantify the potential onshore flows of deep nutrients onto the shelf, which are typical of winter, and the deep wintertime vertical mixing that would bring nutrients to shallow shelf waters.

The budget indicates that advective throughflow of nitrogen in the CGOA is typically quite large relative to other terms. Other regions of the world ocean may experience similarly large "rivers" of nitrate; in particular, the Norwegian Coastal Current. In a

Fig. 15. Modeled horizontal flux (left panel, millimoles $m^{-2} s^{-1}$), vertical advection (middle panel, millimoles $m^{-2} s^{-1} \times 10^3$), and vertical diffusion (right panel, millimoles $m^{-2} s^{-1} \times 10^3$) of nitrate in the vicinity of Amatouli Trough during 1 May 2001. The vectors represent magnitude and direction of nitrate flux, i.e., the velocity vector multiplied by the value of nitrate at that location.
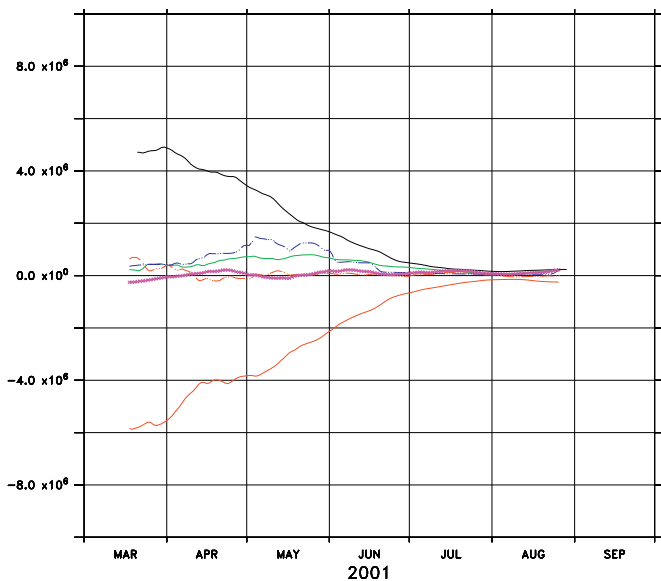

Fig. 16. As in Fig. 14, but for the Amatouli Trough control volume.

Bank. New production appears preferentially along the margins, where strong fronts develop with associated vertical velocities: downwelling on the side facing the bank, and upwelling on the side facing offbank (Franks and Chen, 1996, 2001). As described by Ji et al. (2006), when vertical mixing is large, blooms and associated nutrient depletion occur first in the shallower areas (i.e., on the bank itself), where light is more abundant throughout the vertically mixed water column. Later in the year, as rising incident light deepens the euphotic zone (and the water column begins to stratify, trapping phytoplankton near the surface), progressively deeper areas are subject to blooming. Throughout the summer, frontal circulation, tidal excursion and vertical mixing along the flanks transports nitrogen both upward and onto the bank. This feeds new production and higher chlorophyll levels preferentially at the margins.

It is plausible that similar mechanisms drive the observed toroidal pattern over Portlock Bank, and other submarine banks around the world ocean (e.g., Dogger Bank in the North Sea; Nielsen et al., 1993; Richardson et al., 2000). Note, however, that the CGOA shelf is strongly affected by freshwater runoff, which likely accelerates the bloom off the bank (as it traps phytoplankton near the surface). In other words, early in the growing season, a plausible explanation for the toroidal geometry over Portlock Bank is that intense tidal mixing over the caps of the banks carries phytoplankton so deep as to render them light-limited, relative to more stratified offbank areas. These aspects of CGOA production are being explored in a separate paper.

4.3. Significance of wind-stress curl

A major and unexpected result of the present work is the existence of substantial curl-driven upwelling of nitrate on the CGOA shelf. Rykaczewski and Checkley (2008) have noted the importance of curl-driven upwelling to biological production off the coast of southern California. Using atmospheric reanalysis data, they observed a correlation between local wind-stress curl, observed nutrient levels, and observed/modeled production of fish biomass. A correspondence on interannual timescales

between wind-stress curl on the CGOA shelf and observed/modeled phytoplankton levels has recently been noted (J. Fiechter, pers. commun.). This underscores the significance of curl-driven fluxes to the annual nitrogen budget of the CGOA, along with terms less subject to interannual variability (e.g., tidally driven mixing).

4.4. Known modeling issues and other considerations

Like all models, the ones used here are imperfect. In particular, all of the freshwater forcing schemes explored in Dobbins et al. (2009) produced more density stratification than was observed. Among other factors, we attribute this bias to our inability at 3-km grid resolution to resolve estuaries along the coast, and the failure of standard mixing schemes to account for extra mixing generated by swell (e.g., Langmuir cells). Hence in the results reported here, the spring bloom on the shelf, and related nutrient depletion, likely occur too early in the season, and the supply of nutrients by vertical diffusion is likely to be an underestimate of its true value. It also appears that modeled surface nitrate is overly depleted in the basin by August; hence we are probably underestimating the onshelf flux of nutrients later in the season. We are presently working to formulate an appropriate parameterization of mixing effects to reduce these biases, and refine our budgets. Finally, the regular x–y–z coordinate system is only one of several possible choices for defining a control volume. An alternate approach would be to calculate fluxes into volumes defined by isopycnal surfaces. This can be useful to define a material surface surrounding a water mass, but is less well justified in the presence of strong vertical mixing. The chosen system, based on the top 15 m of the water column has the virtue of simplicity, and a natural interpretation as the euphotic zone.

5. Conclusion

Using coupled circulation and ecosystem models, we have simulated the physical flux of nitrate on the CGOA shelf, and analyzed the resulting patterns. Fluxes of water and nitrate across the 15 m depth horizon on the shelf indicate a patchy pattern of vertical velocity. When the top 15 m of a 300-km-wide swath of the shelf (our primary "control volume") is considered, the model suggests a net upwelling of water and nutrients during spring (March and April). This upwelling is an unexpected result for the CGOA, given its typical characterization as a downwelling-favorable area. Vertical diffusion of nutrients from below 15 m emerges as the biggest source term throughout the growing season, followed in importance by alongshelf horizontal flux of nutrients from the northeast, onshelf flux from the deep basin, and windstress-curl-driven upwelling across the 15 m depth horizon. Collectively these source terms are nearly balanced by alongshelf outflow to the southwest. It remains to be demonstrated precisely how nutrients replenish this deep source in the winter months. This will require an NPZ model that spans multiple years, an appropriate task for ongoing GLOBEC studies.

Acknowledgments

References

Armstrong, F.A.J., Stearns, C.R., Strickland, J.D.H., 1967. The measurement of upwelling and subsequent biological processes by means of the Technicon AutoAnalyzer and associated equipment. Deep-Sea Research 14, 381–389.

Atlas, E.L., Callaway, J.C., Tomlinson, R.D., Gordon, L.I., Barstow, L., Park, P.K., 1971. A practical manual for the use of the Technicon Autoanalyzer for nutrient analysis. Revised. Oregon State University, Corvallis, OR, Technical Report 215, reference no. 71-22.

Bograd, S.J., Stabeno, P.J., Schumacher, J.D., 1994. A census of mesoscale eddies in Shelikof Strait, Alaska during 1989. Journal of Geophysical Research 99, 18,243–18,254.

Brickley, P., Thomas, A.C., 2003. Satellite-measured seasonal and interannual chlorophyll variability in the Northeast pacific and coastal Gulf of Alaska. Deep-Sea Research II 51, 229–245.

Childers, A.R., Whitledge, T.E., Stockwell, D.A., 2005. Seasonal and interannual variability in the distribution of nutrients and chlorophyll-a across the Gulf of Alaska shelf: 1998–2000. Deep-Sea Research II 52, 193–216.

Coyle, K.O., Hinckley, S., Hermann, A.J., Lessard, E., in preparation. Northern Gulf of Alaska simulations of oceanic and shelf ecosystems: refining and tuning an NPZ model embedding in a general circulation model.

Curchitser, E.N., Haidvogel, D.B., Hermann, A.J., Dobbins, E.L., Powell, T.M., Kaplan, A., 2005. Multi-scale modeling of the North Pacific Ocean I: Assessment and analysis of simulated basin-scale variability (1996–2003). Journal of Geophysical Research 110, C11021.

Dobbins, E.L., Hermann, A.J., Stabeno, P.J., 2009. Modeled transport of freshwater from a line-source in the coastal Gulf of Alaska. Deep-Sea Research II 56 (24), 2409–2426.

Dore, J.E., Houlihan, T., Hebel, D.V., Tien, G., Tupas, L., Karl, D.M., 1996. Freezing as a method of sample preservation for the analysis of dissolved inorganic nutrients in seawater. Mar. Chem. 53, 173–185.

Fennel, K., Abbott, M.R., Spitz, Y.H., Richman, J.G., Nelson, D.M., 2003. Impacts of iron control on phytoplankton production in the modern and glacial Southern Ocean. Deep-Sea Research II 50, 833–851.

Franks, P.J.S., Chen, C., 1996. Plankton production in tidal fronts: a model of Georges Bank in summer. Journal of Marine Research 54, 631–651.

Franks, P.J.S., Chen, C., 2001. A 3-D prognostic model study of the ecosystem over Georges Bank and adjacent coastal regions. Part II: Coupled biological and physical model. Deep-Sea Research II 48, 457–482.

Gordon, L.I., Jennings Jr., J.C., Ross, A.A., Krest, J.M., 1993. A suggested protocol for continuous automated analysis of seawater nutrients (phosphate, nitrate, nitrite and silicic acid) in the WOCE Hydrographic program and the Joint Global Ocean Fluxes Study, WOCE Operations Manual, vol. 3: The Observational Programme, Section 3.2: WOCE Hydrographic Programme, Part 3.1.3: WHP Operations and Methods. WHP Office Report WHPO 91-1; WOCE Report no. 68/91. November, 1994, Revision 1, Woods Hole, MA, USA, 52 loose-leaf pages.

Hermann, A.J., Stabeno, P.J., 1996. An eddy-resolving model of circulation on the western Gulf of Alaska shelf.1. Model development and sensitivity analyses. Journal of Geophysical Research—Oceans 101, 1129–1149.

Hermann, A.J., Curchitser, E.N., Dobbins, E.L., Haidvogel, D.B., 2009. A comparison of remote versus local influence of El Niño on the coastal circulation of the Northeast Pacific. Deep-Sea Research II 56 (24), 2427–2443.

Hinckley, S., Coyle, K.O., Gibson, G., Hermann, A.J., Dobbins, E.L., 2009. A biophysical NPZ model with iron for the Gulf of Alaska: Reproducing the differences between an oceanic HNLC ecosystem and a classical northern temperate shelf ecosystem. Deep-Sea Research II 56 (24), 2520–2536.

Ji, R., Chen, C., Franks, P.J.S., Townsend, D.W., Durbin, E.G., Beardsley, R.C., Lough, R.G., Houghton, R.W., 2006. Spring phytoplankton bloom and associated lower trophic food web dynamics on Georges Bank: 1-D and 2-D model studies. Deep-Sea Research II 53, 2656–2683.

Ladd, C., Stabeno, P., Cokelet, E.D., 2005a. A note on cross-shelf exchange in the northern Gulf of Alaska. Deep-Sea Research II 52, 667–679.

Ladd, C., Kachel, N.B., Mordy, C.W., Stabeno, P.J., 2005b. Observations from a Yakutat eddy in the northern Gulf of Alaska. Journal of Geophysical Research—Oceans 110, C03003.

Large, W.G., McWilliams, J.C., Doney, S.C., 1994. Oceanic vertical mixing—a review and a model with a nonlocal boundary-layer parameterization. Reviews of Geophysics 32, 363–403.

Martin, J.H., Gordon, R.M., Fitzwater, S., Broenkow, W.W., 1989. VERTEX: phytoplankton/iron studies in the Gulf of Alaska. Deep-Sea Research A 36, 649–680.

Nielsen, T.G., Løkkegaard, B., Richardson, K., Bo Pedersen, Fl., Hansen, L., 1993. The structure of the plankton communities in the Dogger Bank Area (North Sea) during a stratified situation. Marine Ecology Progress Series 95, 115–131.

OCSEAP Staff, 1987. Marine fisheries: resources and environment. In: Hood, D.W., Zimmerman, S.T. (Eds.), The Gulf of Alaska Physical Environment and Biological Resources. US Minerals Management Service, Springfield, VA, pp. 417–458.

Okkonen, S.R., Weingartner, T.J., Danielson, S.L., Musgrave, D.L., Schmidt, G.M., 2003. Satellite and hydrographic observations of eddy-induced shelf-slope exchange in the northwestern Gulf of Alaska. Journal of Geophysical Research—Oceans 108 (C2), 3033.

Proctor, R., Holt, J.T., Allen, J.I., Blackford, J., 2003. Nutrient fluxes and budgets for the North West European Shelf from a three-dimensional model. Science of the Total Environment 314-316, 769–785.

Richardson, K., Visser, A., Pedersen, Fl.B., 2000. Subsurface phytoplankton blooms fuel summer production in the North Sea. Journal of Plankton Research 22 (9), 1663–1671.

Royer, T.C., 1998. Coastal processes in the northern North Pacific. In: Robinson, A.R., Brink, K.H. (Eds.), The Sea. Wiley, New York, pp. 395–414.

Rykaczewski, R.R., Checkley, D.M., 2008. Influence of ocean winds on the pelagic ecosystem in upwelling regions. Proceedings of the National Academy of Sciences of the United States of America 105, 1965–1970.

Sambrotto, R.N., Lorenzen, C.J., 1987. Phytoplankton and primary production. In: Hood, D.W., Zimmerman, S.T. (Eds.), The Gulf of Alaska: Physical Environment and Biological Resources. US Department of Commerce, USA, pp. 249–282.

Skogen, M.D., Svendsen, E., Berntsen, J., Aksnes, D., Ulvestad, K., 1995. Modelling the primary production in the North Sea using a coupled three-dimensional physical–chemical–biological ocean model. Estuarine, Coastal and Shelf Science 41, 545–565.

Skogen, M.D., Budgell, W.P., Rey, F., 2007. Interannual variability in Nordic seas primary production. ICES Journal of Marine Science 64, 889–898.

Stabeno, P.J., Hermann, A.J., 1996. An eddy-resolving model of circulation on the western Gulf of Alaska shelf. 2. Comparison of results to oceanographic observations. Journal of Geophysical Research—Oceans 101, 1151–1161.

Stabeno, P.J., Bond, N.A., Hermann, A.J., Kachel, N.B., Mordy, C.W., Overland, J.E., 2004. Meteorology and oceanography of the Northern Gulf of Alaska. Continental Shelf Research 24, 859–897.

Strom, S.L., Olson, M.B., Macri, E.L., Mordy, C.W., 2006. Cross-shelf gradients in phytoplankton community structure, nutrient utilization, and growth rate in the northern coastal Gulf of Alaska. Marine Ecology Progress Series 328, 75–92.

Williams, W.J., 2003. Idealized modeling of seasonal variation in the Alaska Coastal Current. Ph.D. Thesis, University of Alaska, Fairbanks, 100pp.

Williams, W.J., Weingartner, T.J., Hermann, A.J., 2007. Idealized three-dimensional modeling of seasonal variation in the Alaska Coastal Current. Journal of Geophysical Research 112, C07001.

Weingartner, T.J., Coyle, K.O., Finney, B., Hopcroft, R., Whitledge, T.E., Brodeur, R., Dagg, M., Farley, E., Haidvogel, D.B., Haldorson, L., Hermann, A.J., Hinckley, S., Napp, J., Stabeno, P.J., Kline, T., Lee, C., Lessard, E., Royer, T.C., Strom, S., 2002. The Northeast Pacific GLOBEC Program: Coastal Gulf of Alaska. Oceanography 15, 48–63.